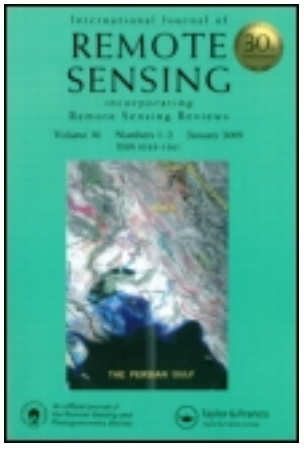

International Journal of Remote Sensing

Publication details, including instructions for authors and subscription information:
http://www.tandfonline.com/loi/tres20

Spatial variability of frontal area index and its relationship with urban heat island intensity

Man Sing Wong [a] & Janet E. Nichol [a]

[a] Department of Land Surveying and Geo-Informatics, The Hong Kong Polytechnic University, Hunghom, Kowloon, Hong Kong

Version of record first published: 02 Oct 2012.

To cite this article: Man Sing Wong & Janet E. Nichol (2013): Spatial variability of frontal area index and its relationship with urban heat island intensity, International Journal of Remote Sensing, 34:3, 885-896

To link to this article: http://dx.doi.org/10.1080/01431161.2012.714509

International Journal of Remote Sensing
Vol. 34, No. 3, 10 February 2013, 885–896

Taylor & Francis
Taylor & Francis Group

Spatial variability of frontal area index and its relationship with urban heat island intensity

Man Sing Wong* and Janet E. Nichol

Department of Land Surveying and Geo-Informatics, The Hong Kong Polytechnic University, Hunghom, Kowloon, Hong Kong

(*Received 20 April 2011; accepted 27 September 2011*)

In densely urbanized regions, the local climate is greatly influenced by the urban morphology, including interactions between buildings, space, and human activities. The Kowloon Peninsula in Hong Kong, with some of the greatest urban population densities in the world, represents an extreme case of the influence of the built environment on climate, with high-rise buildings, narrow street canyons, and little green space. In this study, the building frontal area index (FAI), a parameter for estimating aerodynamic resistance of the urban surface as a predictor of wind ventilation, was derived from a three-dimensional building database. The relationship between FAI and urban heat island intensity (UHII) from an Advanced Spaceborne Thermal Emission and Reflection Radiometer (ASTER) satellite image was calculated at different scales. The highest correlation ($r = 0.574$, $n = 4900$) was obtained at 100 m resolution, which suggests that the optimum operational scale of FAI is 100 m resolution for the study area, i.e. the scale and size at which FAI impacts on the urban climate. The presence/trend of any higher correlation at different resolutions was tested using the nonparametric Mann–Kendall test, and the results show that the statistic Z-value generated from the test is smaller than the hypothesis significance levels of 90%, 95%, and 99%; thus, the hypothesis of having a higher correlation at any scale other than 100 m resolution is rejected. Planning authorities may use the FAI generated at 100 m resolution for designing wind ventilation corridors across Hong Kong at this scale, especially when temperature and air quality in the inner city are of major concern. However, for applications to other cities with different standard morphologies, the FAI–UHII relationship should be re-evaluated.

1. Introduction

The urban heat island (UHI) refers to the difference in air temperature between urban and rural areas. The main causes are the increased use of impervious land surfaces covered by artificial materials, the density of construction, and the removal of vegetation cover, as well as anthropogenic heat discharge due to human activities.

Heat islands have adverse health impacts (Changnon, Kunkel, and Reinke 1996; McMichael 2000; CDC 2006; Robine et al. 2008), reduce work efficiency, and result in high energy consumption for air conditioning (Akbari 2005), especially in tropical cities such as Hong Kong. Air-conditioning exhausts contribute to the heating of a city, thereby requiring more air conditioning. Heat accumulated by the urban built structures during the day can to some extent be removed or mitigated by effective ventilation (Yim et al. 2009; Wong et al. 2010).

*Corresponding author. Email: m.wong06@fulbrightmail.org

ISSN 0143-1161 print/ISSN 1366-5901 online

http://dx.doi.org/10.1080/01431161.2012.714509
http://www.tandfonline.com

Since the UHI is a city-scale phenomenon, remote sensing is the only data-collection method that indicates its full extent over whole cities, using land surface temperature (T_s) derived from satellite images (Balling and Brazel 1988; Quattrochi and Ridd 1994; Lo, Quattrochi, and Luvall 1997; Dousset and Gourmelon 2003; Nichol and Wong 2008; Nichol et al. 2009; Wong, Nichol, and Lee 2010). In addition, urban heat island intensity (UHII), a more objective and absolute measure of heat island magnitude, can also be derived from these images (Equation (1)) if a significant relationship between T_s and air temperature (T_a) can be established.

$$\text{UHII} = T_a \text{ in city centre} - T_a \text{ in rural areas.} \quad (1)$$

Measures that prevent and mitigate heat island formation, such as providing adequate green space and ventilation, are applicable to any city, but the scale at which they are applied is dependent on an individual city's form or structure. Modelling wind ventilation at a variety of scales, from local-street-canyon scale up to the scale of a whole city provides specific locational information on air movement in relation to the built structure and surrounding space of any particular city. Wind ventilation models from computational fluid dynamics (CFD) and wind tunnels provide ideal data for advancing this area of the discipline. However, CFD models are limited to meso-scale operation and can only predict temperature and wind flow in an urban district of hundreds of buildings, which cannot be extended to a large urban area such as the entire Kowloon Peninsula due to its high computer demands. Wind tunnel models provide an alternative for visualizing the local wind direction and pollutant dispersion at large scales over a district but they are also limited to small area coverage with high computer processing requirements and high operational cost.

The frontal area index (FAI) model (Grimmond and Oke 1999; Burian, Brown, and Linger 2002) was devised for representing the surface roughness in urban areas for input to urban climate models. Wong et al. (2010) used derived FAI from three-dimensional geographical information system (GIS) building data to model ventilation corridors across Hong Kong's urban area, and compared the results subjectively with UHI distribution. The FAI was found to have a certain degree of agreement with UHII; however, the spatial variability of FAI and the approximate optimal resolution of FAI related to UHII at city-scale study are still unknown. If the scale at which better ventilation could effect a reduction in heat island formation were known, it would enable planners to design urban districts with better penetration of cool fresh air. In a densely urbanized and populated study area like the Kowloon Peninsula in Hong Kong, urban canyons are narrow, building structures are complex, and there is little integral space. The aims of this article are then (i) to analyse the relationship between FAI and UHII at different scales and (ii) to find the optimum operational scale and resolution of FAI, i.e. the scale and size at which it interacts most strongly with heat island intensity.

2. Study area and data used

The Kowloon Peninsula in Hong Kong, an urban area with tropical climate, has suffered from the urban heat island effect for three decades. A heat island magnitude of 7–8°C is suggested by a recent night-time Advanced Spaceborne Thermal Emission and Reflection Radiometer (ASTER) satellite image of Hong Kong, which is confirmed by simultaneous *in situ* ground data of surface and air temperatures (Nichol et al. 2009), recorded at the image time.

Three-dimensional GIS data of building polygons at 1:5000 scale were input to a program written in ESRI® ArcGIS™ 9.2 software to estimate the total frontal area in the projected plane normal to the specific wind direction (Wong et al. 2010). The FAI is calculated by measurement of building walls facing the wind flow in a particular direction (frontal area per unit horizontal area). The FAI so derived has a strong relationship with the urban surface roughness, and influences the flow regime within urban street canyons (Burian, Brown, and Linger 2002). An ASTER satellite image, which shows the typical urban heat island distribution over the city, was also acquired on 31 January 2007 (around 10:42 pm local time). The low wind speeds observed in inner areas of the Kowloon Peninsula were $\sim$0.5 m s^{-1} during the image acquisition time (both at the MongKok roadside and ShamShuiPo general stations) – these two areas represent heat island core areas in Kowloon (Nichol and Wong 2005; Nichol 2009; Nichol et al. 2009). In addition, low humidity of 55% and a temperature inversion below 600 m altitude were observed during image acquisition.

3. Methodology

The FAI is derived from the total area of building facets projected to plane normal facing a particular wind direction divided by the plane area (Equation (2)) (Figure 1):

$$\mathrm{FAI} = \frac{\mathrm{Area}_{\mathrm{facets}} Z_{\mathrm{mean\ lot}}}{\mathrm{Area}_{\mathrm{lot}}}, \tag{2}$$

where $\mathrm{Area}_{\mathrm{facets}}$ is the total area of building facets facing the wind direction, $\mathrm{Area}_{\mathrm{lot}}$ is the lot area, and $Z_{\mathrm{mean\ lot}}$ is the mean height of the lot area. If FAI $\geq$ 1.0, this means that wind is mostly blocked by buildings within a selected plane region (e.g. $\mathrm{Area}_{\mathrm{facets}} \geq \mathrm{Area}_{\mathrm{lot}}$); if FAI $\sim$ 0.5, it means that wind is half blocked (e.g. $2\mathrm{Area}_{\mathrm{facets}} \approx \mathrm{Area}_{\mathrm{lot}}$); and if FAI = 0, it means that there is no building inside the grid. We modified the algorithm of Burian, Brown, and Linger (2002) in that we only considered the first windward facet in the program, whereas the algorithm of Burian, Brown, and Linger (2002) considered every

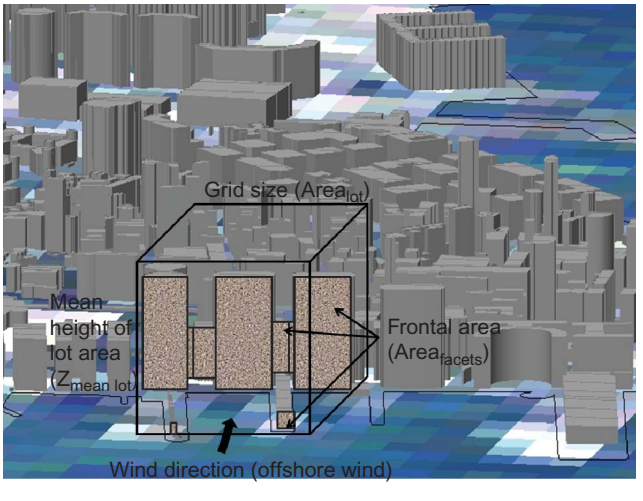

Figure 1. Urban surfaces for the calculation of frontal area index.

windward facet (i.e. all walls having the same aspect). Therefore, their frontal area values are expected to be much higher than ours. In a densely built environment like Hong Kong, the inclusion of only the first windward facet should be more meaningful than including all other windward facets blocked by the first building, because (i) wall-effect buildings are significant in Hong Kong (wall-effect buildings are those high-rise buildings orientated parallel to the coast and blocking most of the onshore winds, thus those buildings behind wall-effect buildings suffer from poor ventilation); (ii) the high density of building blocks in Hong Kong, where most of the winds are blocked by the first windward building, and the second or third buildings are always shielded. Thus, only the first windward facet is counted in our frontal area calculation. The program written in ESRI ArcGIS 9.2 software first generates projected lines in the wind direction with a 3 m horizontal increment, and the particular wind direction is input by the user. When the projected lines hit the first facet of a building, the frontal area of the first facet will only be calculated. If some areas on the second facet of other buildings are not blocked by the first building, these areas will also be included in $\text{Area}_{\text{facets}}$ during the calculation. The calculated frontal areas are then regrouped based on horizontal plane polygons (e.g. grid cell from 40 to 400 m). The method suggested in this study has the advantage when dealing with irregular building groups, as it only considers the area of windward facets, and thus can reduce the number of facets being calculated in the computer memory. More details are given in Wong et al. (2010).

The FAI grid surfaces were computed from 40 to 400 m at grid size intervals of 20 m for eight different wind directions individually. A computer cluster network was set up to operate this program since it is highly computer demanding, especially for small grid sizes. The maximum grid size was 400 m, because this approximates the typical size of urban districts in Kowloon Peninsula. Figure 2 shows the distribution of FAI values averaged for eight different wind directions (north, northeast, east, southeast, south, southwest, west, and northwest), at (*a*) the highest (40 m) and (*b)* the lowest (400 m) resolutions. The 'averaged' images were only for illustration and the actual east direction of FAI was used for comparison with UHII since easterly wind was observed at the image time (around 10:42 pm local time on 31 January 2007). The easterly and northeasterly winds are typical wind directions in Hong Kong, and they account for 66% of all the winds throughout the year (Wong, Nichol, and Lee 2010).

First, the ASTER satellite image with a spatial resolution of 90 m was orthorectified using the rational function model (RFM) with 35 well-identified ground control points (GCPs) distributed over the study area. The GCPs were selected from high-contrast features on the 1:5000 GIS road and building layers. The root mean square error (RMSE) for the GCPs was approximately half a pixel for both east–west and north–south directions. Secondly, radiometric and emissivity corrections were applied for converting the spectral radiance to the brightness temperature (BT) and emissivity-corrected surface temperature. The emissivity modulation method by Nichol (2009) aims to enhance the spatial resolution of thermal satellite images, while simultaneously correcting the image-derived temperatures for emissivity corrections (Nichol 1994, 2005; Nichol et al. 2007). The rationale is to fuse higher resolution (e.g. 10 m) emissivity values from a land-cover map with lower resolution (e.g. 90 m) thermal images based on the assumption that temperatures within a large pixel vary only by cover type. Figure 3 shows the land-cover map acquired from the Hong Kong Planning Department and regrouped into six major classes, namely forest, grassland, shrubland, water, urban, and soil/sand. The emissivity-modulation method then allocates emissivity values to each land-cover type for input to Equation (3) (Sabins 1997):

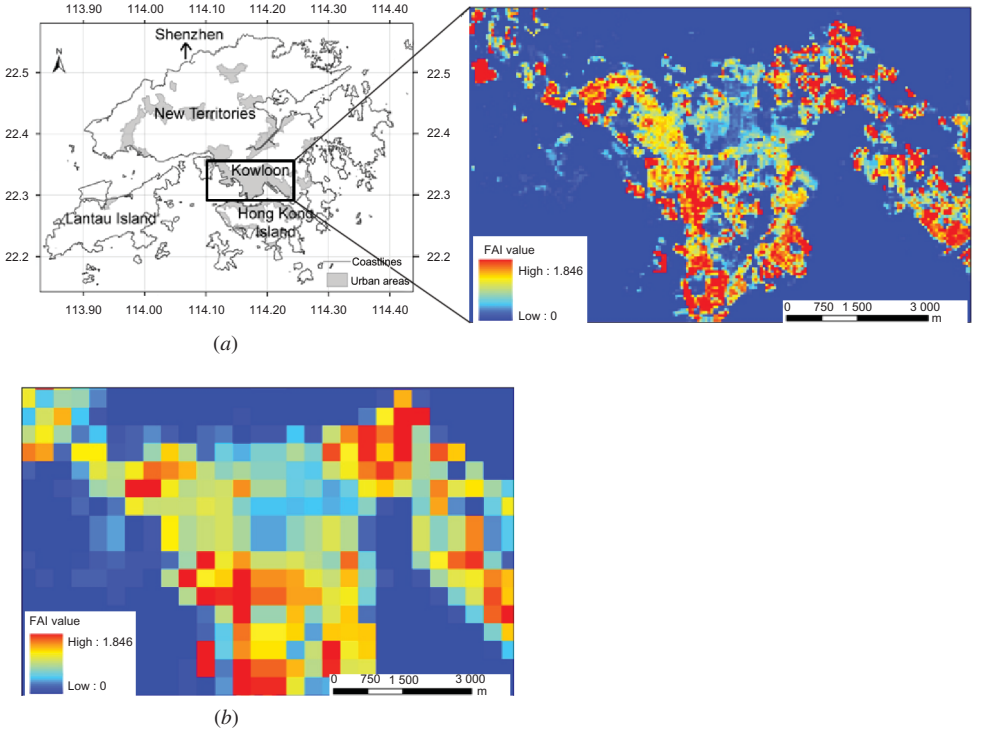

Figure 2. Averaged frontal area index at eight different directions: (*a*) at 40 m resolution and (*b*) at 400 m resolution.

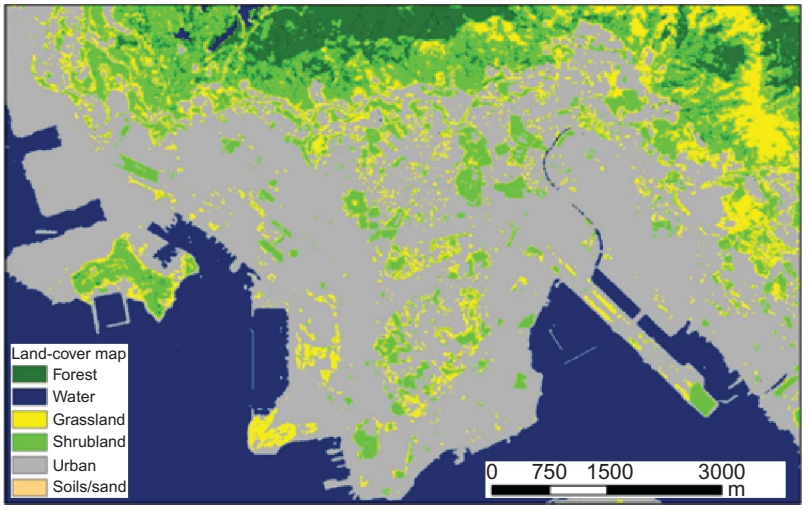

Figure 3. Land-cover map of study area.

$$T_s = \frac{T_b}{\varepsilon^{1/4}}, \tag{3}$$

where T_s is the land surface temperature, T_b is the black body temperature, and ε is the emissivity value. The derived T_s image is at 10 m spatial resolution (Nichol 2009).

Thirdly, the ASTER T_s image was converted to air temperature (T_a) using the relationship between field-measured air and surface temperature (Fung et al. 2009). Atmospheric correction for the ASTER T_s image was carried out by comparing the pixel value with the known sea surface temperature (SST) (Nichol 2005). This is because the derived ASTER T_s image gives a limited range of surface temperatures, over which atmospheric absorption should be linear. Eighteen paired field surface (T_s) and air temperatures (T_a) were recorded in both urban and rural areas across Hong Kong territories, within 1.5 hours of the image time, 10:42 pm local time. The air temperatures T_a were measured 1 m from the ground surface using Testo 720 portable digital thermometers with air and contact surface probes, having a stated accuracy of 0.2°C, and each measurement representing the average of three readings. The thermometers were first calibrated using an Omega CL730A calibrator and a certified mercury thermometer NIST SRM943 before field work. Through the relationship between 18 pairs of field T_a and image T_s (these are extracted from geometric, radiometric, emissivity, and atmospheric-corrected images at 10 m resolution), the image T_a can be derived as in Equation (4).

$$\text{field } T_a = 0.99 \text{ image } T_s - 1.63, \tag{4}$$

where this relationship can be applied to all pixels for deriving image T_a, by substituting image T_a to field T_a in Equation (4).

A strong correlation ($r = 0.824$) and low standard deviation (SD = 1.719) were observed between the ASTER image temperatures and field air temperatures at the image time due to a strong inversion and stable atmospheric boundary condition on the night of the image acquisition. Finally, the UHII image was derived from image T_a using Equation (1).

In order to investigate the spatial variability of FAI in relation to UHII, the UHII values were spatially averaged at decreasing resolutions from 40 to 400 m similar to the FAI resolutions computed. Figure 4 shows the (*a*) UHII and (*b*) FAI at different resolutions.

In order to test the optimum scale of correspondence between FAI and UHII, the correlation coefficient and the Mann–Kendall test were used. As grid sizes increase, the surface types within each grid cell would be expected to be more heterogeneous and the correlation between FAI and UHII may be expected to fall. The correlation would also fall if the UHII became too generalized at larger grid sizes and was more dependent on city-scale processes than on local morphology. The Mann–Kendall test was used to examine whether there is a significant tendency/trend of increasing correlation between FAI and UHII when the resolution is degraded (from 40 to 400 m, with an interval of 20 m). This test is based on a set of hypotheses to examine the relations between a set of observations (Mann 1945; Kendall 1975). The test first compares each resolution/scale with the others in sequential order, and the number of times with larger, smaller, and equal values is counted (Equations (5) and (6)):

$$S = \sum_{j=1}^{n-1} \sum_{i=j+1}^{n} \text{sign}(x_i - x_j), \tag{5}$$

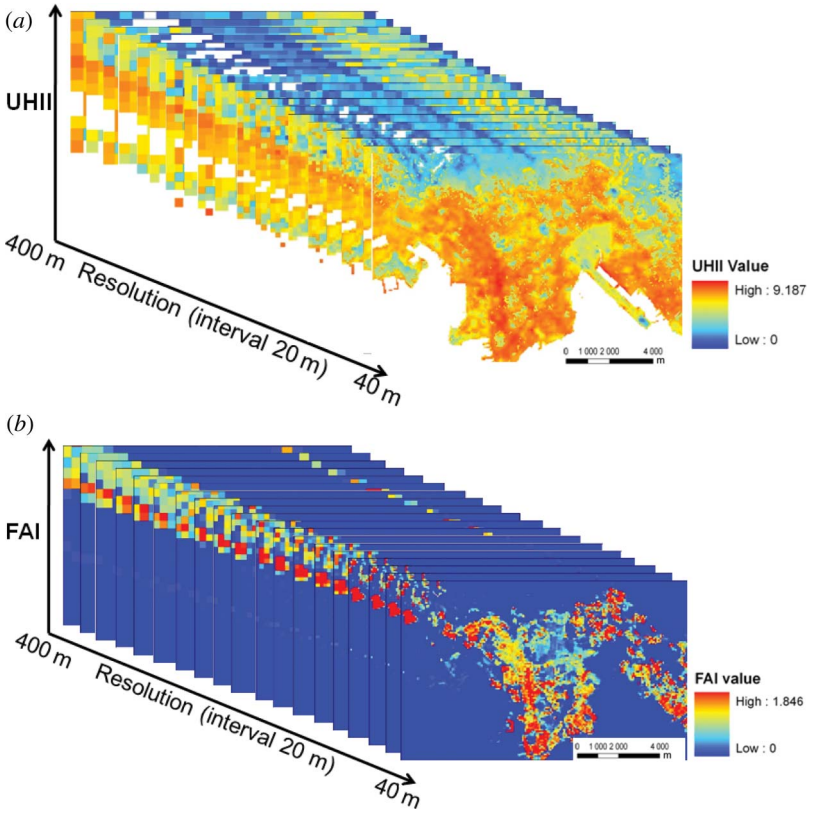

Figure 4. (*a*) Urban heat island intensity and (*b*) frontal area index at different resolutions.

$$\text{sign}(x_i - x_j) = \begin{cases} 1, & \text{if } (x_i - x_j) > 0 \\ 0, & \text{if } (x_i - x_j) = 0 \\ -1, & \text{if } (x_i - x_j) < 0 \end{cases}, \tag{6}$$

where n is the number of observations (e.g. 19 resolutions in this study), x_i and x_j are two sequential data values (i.e. when x_i = correlation at 60 m, x_j = correlation at 40 m, and when x_i = correlation at 80 m, x_j = correlation at 60 m). Each correlation between UHII and FAI at each resolution is compared with all other subsequent correlations at different resolutions. If a correlation from lower resolution is higher than a correlation from higher resolution, S is incremented by 1. If a correlation from lower resolution is smaller than higher resolution, S is decremented by 1. The net result of all increments and decrements produces the final value S.

Kendall (1975) describes a normal-approximation test for data sets with more than 10 values. The expected mean value and variance of S can be derived from Equations (7) and (8):

$$E(S) = 0, \tag{7}$$

$$\mathrm{Var}(S) = \frac{\left[n(n-1)(2n+5) - \sum_t t(t-1)(2t+5)\right]}{18}, \tag{8}$$

where t is the number of ties (e.g. the correlations are exactly the same inside the sequence of resolutions from 40 to 400 m), and the second term represents an adjustment for tied or censored data. Finally, the normalized test statistic Z can be calculated using Equation (9):

$$Z = \begin{cases} \dfrac{S-1}{\sqrt{\mathrm{Var}(S)}}, & \text{if } S > 0 \\ 0, & \text{if } S = 0 \\ \dfrac{S-1}{\sqrt{\mathrm{Var}(S)}}, & \text{if } S < 0 \end{cases}. \tag{9}$$

The Z-value is used to test the presence/absence of the trend. A positive Z-value indicates an increasing trend of having higher correlations when resolution is degraded and a negative Z-value indicates a decreasing trend of having lower correlations when resolution is degraded. $Z = 0$ when no trend is observed. The hypothesis of significant trend (either increasing or decreasing) is accepted if the following condition (Equation (10)) applies:

$$|Z| > U_\alpha,$$

where the significant level (α) in a normal distribution (U) is the threshold of probability which should be set before the test, e.g. 90%, 95%, and 99%.

4. Results

The highest correlation between FAI and UHII appears to be at the scale of 100 m, with a correlation coefficient value of $r = 0.574$ ($n = 4900$) (Figure 5). The peak at 100 m may be related to 100 m being approximately the upper threshold limit for the operation of small-scale turbulence (Oke 1987) at the urban-canyon scale, and its replacement by meso-scale processes at city-block scale. In addition, resolution of 100 m is probably a typical urban canopy packing density (Barlow and Coceal 2009) and this resolution was used in the full-scale flux observations in Vancouver (Schmid et al. 1991).

The Z-value generated from the Mann–Kendall test (1.609) is smaller than the hypotheses significance levels of 90%, 95%, and 99% (1.645, 1.960, and 2.576) (Table 1), respectively, indicating that the hypothesis of having a significant tendency/trend from 40 to 400 m resolution is rejected. Since 100 m is found to have the highest correlation among all 19 resolutions, another similar Mann–Kendall test was applied to resolutions beyond 100 m for testing for a significant trend from 100 to 400 m. The resulting Z-value in Table 2 shows a smaller value than the hypotheses significance levels of 90%, 95%, and 99%, indicating that the hypothesis of a significant trend and higher correlation at any scale other than 100 m resolution is rejected. Thus, there is no higher correlation observed between FAI and UHII when the resolution is decreased from the scale of 400 m.

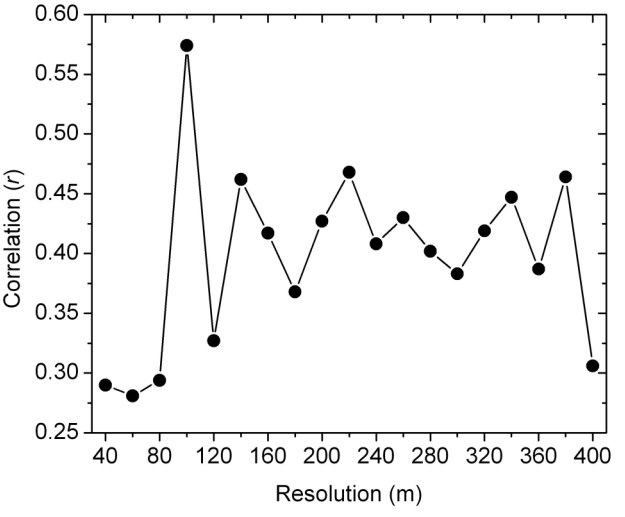

Figure 5. Correlations between frontal area index and urban heat island intensity at different resolutions.

Table 1. Results of the Mann–Kendall test (trend hypothesis test) using a whole set of data (resolution from 40 to 400 m).

Significant level in hypothesis test (α)	Mann–Kendall generated Z-value	Accept/reject
1.645 (90%)	1.609	Reject (no significant trend)
1.960 (95%)	1.609	Reject (no significant trend)
2.576 (99%)	1.609	Reject (no significant trend)
n (number of samples)	19	

Table 2. Results of Mann–Kendall test using data beyond 100 m resolution (from 100 to 400 m).

Significant level in hypothesis test (α)	Mann–Kendall generated Z-value	Accept/reject
1.645 (90%)	−0.045	Reject (no significant trend)
1.960 (95%)	−0.045	Reject (no significant trend)
2.576 (99%)	−0.045	Reject (no significant trend)
n (number of samples)	16	

5. Conclusion and discussion

The simple method presented here for estimating aerodynamic resistance and wind ventilation using FAI is a promising approach for evaluating the relationship between the urban heat island and wind penetration in densely built cities. The optimal resolution of the FAI was found to be 100 m and this was able to explain 57.4% of the variance in the heat island intensity map. This appears logical and reasonable, since FAI is based on building area footprints and heights, and thus it corresponds closely to built volume across the urban area, which is comparable to other heat island-related parameters such as the sky view factor. The remaining 42.6% of the variance not explained at the 100 m scale may be due to factors

other than those that are related to geometric form, such as variations in anthropogenic heat generated in the city and heat loss from different types of surface materials. Although only moderate, this correlation is significantly higher than correlations obtained between FAI and other urban environmental parameters such as aerosol optical thickness (0.251), the normalized difference vegetation index (NDVI) (–0.449), building density (0.522), and building height (0.383) observed in another study (Wong et al. 2010).

The observation of similarity between the optimal resolution (100 m) in this study and the ASTER original 90 m thermal image can be found. But according to Nichol (2009), the emissivity-corrected image at higher resolution (e.g. 10 m) has a better relationship with ground measurements ($r = 0.72$) than the original image at 90 m resolution ($r = 0.31$). The lower accuracy of T_s at 90 m resolution is attributed to the mixed pixel problem, especially in urban areas with fragmented land cover. Thus, the higher resolution of the emissivity-corrected image appears to provide a better description of large-scale variability of surface and air temperature in Hong Kong. The highest correlation at 100 m is thought to be due to the strong relationship between the city's geometric structure and the intensity of the urban heat island.

Although only one satellite image is used in this study for evaluating the relationship between UHII with FAI, To, Nichol, and Tse (2011) show that thermal satellite images of Hong Kong are able to represent air temperatures over the Kowloon Peninsula within ± 2 hours of the image time during the day and ± 5 hours at night. To, Nichol, and Tse (2011) also show that the spatial patterns of air temperatures represented by the thermal images are similar to other days/nights when atmospheric conditions are similar (e.g. stable boundary layer and low wind conditions). Strong correlations between image-derived air temperatures and station-recorded air temperatures (from Hong Kong Observatory) were observed in other satellite images (linear correlation of 0.79 and 0.84 on 22 August 2009, 11 am local time, and 13 August 2008, 10 pm local time, respectively). In this study, a strong correlation is observed between air and surface temperatures during a night with a stable boundary layer and low wind conditions, which is common at night-time in Hong Kong.

The optimum resolution (100 m) of FAI observed here suggests that ventilation corridors of 100 m width would be suitable for city-scale planning to mitigate heat island formation. A similar study in Cairo, Egypt, also demonstrated that the most significant and applicable resolution of FAI was between 75 and 125 m (Frey and Parlow 2010). More studies will be conducted to model the roughness parameters of vegetation, because although urban vegetation on the Kowloon Peninsula is small and fragmented, and is small compared to the roughness of buildings, evapotranspiration by trees can provide significant cooling effects in a city.

Acknowledgments

This project was funded by the Public Policy Research Project PPR-K-QZ04 and PolyU FCLU Sustainable Urbanization Research Fund (SURF) (1-ZV4V). The authors acknowledge Mr Pui Hang To for data processing.

References

Akbari, H. 2005. Energy Saving Potentials and Air Quality Benefits of Urban Heat Island Mitigation, *Report from Lawrence Berkeley National Laboratory*, US. Accessed June 29, 2011. http://www.osti.gov/bridge/servlets/purl/860475-UlHWIq/860475.PDF.

Balling, R. C., and S. W. Brazel. 1988. "High Resolution Surface Temperature Patterns in a Complex Urban Terrain." *Photogrammetric Engineering and Remote Sensing* 54: 1289–93.

Barlow, J. F., and O. Coceal. 2009. *A Review of Urban Roughness Sublayer Turbulence. UK Meteorology Research and Development*, *Meteorology Office Technical Report 527*, Department of Meteorology, Reading University, UK.

Burian, S. J., M. J. Brown, and S. P. Linger. 2002. *Morphological Analysis Using 3D Building Databases, Los Angeles, CA. LA-UR-02-0781*, 36–42. Los Alamos, NM: Los Alamos National Laboratory.

CDC. 2006. *Extreme Heat: A Prevention Guide to Promote Your Personal Health and Safety. Report from Center for Disease Control and Prevention*, US. Accessed June 29, 2011. http://www.bt.cdc.gov/disasters/extremeheat/heat_guide.asp.

Changnon, S. A., K. E. Kunkel, and B. C. Reinke. 1996. "Impacts and Responses to the 1995 Heat Wave: A Call to Action." *Bulletin of the American Meteorological Society* 77: 1497–506.

Dousset, B., and F. Gourmelon. 2003. "Satellite Multi-Sensor Data Analysis of Urban Surface Temperatures and Land Cover." *ISPRS Journal of Photogrammetry and Remote Sensing* 58: 43–54.

Frey, C. M., and E. Parlow. 2010. "Determination of the Aerodynamic Resistance to Heat Using Morphometric Methods." *EARSeL eProceedings* 9: 52–63.

Fung, W. Y., K. S. Lam, J. E. Nichol, and M. S. Wong. 2009. "Heat Island Study – Satellite Derived Air Temperature." *Journal of Applied Meteorology and Climatology* 48: 863–72.

Grimmond, C. S. B., and T. R. Oke. 1999. "Aerodynamic Properties of Urban Areas Derived from Analysis of Surface Form." *Journal of Applied Meteorology* 34: 1262–92.

Kendall, M. G. 1975. *Rank Correlation Measures*. London: Charles Griffin.

Lo, C. P., D. A. Quattrochi, and J. C. Luvall. 1997. "Applications of Thermal Infra-Red Remote Sensing and GIS to Assess the Urban Heat Island Effect." *International Journal of Remote Sensing* 18: 287–304.

Mann, H. B. 1945. "Nonparametric Tests against Trend." *Econometrica* 13: 245–59.

Mcmichael, A. J. 2000. "The Urban Environment and Health in a World of Increasing Globalization: Issues for Developing Countries." *Bulletin of the World Health Organization* 78: 1117–26.

Nichol, J. E. 1994. "A GIS Based Approach to Microclimate Monitoring in Singapore's High Rise Housing Estates." *Photogrammetric Engineering and Remote Sensing* 60: 1225–32.

Nichol, J. E. 2005. "Remote Sensing of Urban Heat Islands by Day and Night." *Photogrammetric Engineering and Remote Sensing* 71: 613–21.

Nichol, J. E. 2009. "An Emissivity Modulation Method for Spatial Enhancement of Thermal Satellite Images in Urban Heat Island Analysis." *Photogrammetric Engineering & Remote Sensing* 75: 547–56.

Nichol, J. E., W. Y. Fung, K. S. Lam, and M. S. Wong. 2009. "Urban Heat Island Diagnosis Using ASTER Satellite Images and 'In Situ' Air Temperature." *Atmospheric Research* 94: 276–84.

Nichol, J. E., B. A. King, D. Quattrochi, I. Dowman, M. Ehlers, and X. Ding. 2007. "Policy Document on Earth Observation for Urban Planning and Management." *Photogrammetric Engineering and Remote Sensing* 73: 973–9.

Nichol, J. E., and M. S. Wong. 2005. "Modelling Urban Environmental Quality in a Tropical City." *Landscape and Urban Planning* 7: 49–58.

Nichol, J. E., and M. S. Wong. 2008. "Spatial Variability of Air Temperature over a City on a Winter Night." *International Journal of Remote Sensing* 29: 7213–23.

Oke, T. R. 1987. *Boundary Layer Climates*. 2nd ed. Methuen, MA: Taylor & Francis.

Quattrochi, D. A., and M. K. Ridd. 1994. "Measurement and Analysis of Thermal Energy Responses from Discrete Urban Surfaces Using Remote Sensing Data." *International Journal of Remote Sensing* 15: 1991–2002.

Robine, J.-M., S. L. K. Cheung, S. Le Roy, H. Van Oyen, C. Griffiths, J.-P. Michel, and F. R. Herrmann. 2008. "Death Toll Exceeded 70,000 in Europe During the Summer of 2003." *Comptes Rendus Biologies* 331: 171–8.

Sabins, F. F. 1997. *Remote Sensing: Principles and Interpretation*. 3rd ed. New York: W.H. Freeman.

Schmid, H. P., H. A. Cleugh, C. S. B. Grimmond, and T. R. Oke. 1991. "Spatial Variability of Energy Fluxes in Suburban Terrain." *Boundary-Layer Meteorology* 54: 249–76.

To, P. H., J. E. Nichol, and R. Tse. 2011. "Temporal Characteristics of Thermal Satellite Images for Urban Climate Study." In: *Proceedings of Urban Remote Sensing Event (JURSE)*, Munich, April 11–13, 2011, 137–140.

Wong, M. S., J. E. Nichol, and K. H. Lee. 2010. "A Satellite View of Urban Heat Island: Causative Factors and Scenario Analysis." *Korean Journal of Remote Sensing* 26: 617–27.

Wong, M. S., J. E. Nichol, P. H. To, and J. Z. Wang. 2010. "A Simple Method for Designation of Urban Ventilation Corridors and Its Application to Urban Heat Island Analysis." *Building and Environment* 45: 1880–9.

Yim, S. H. L., J. C. H. Fung, A. K. H. Lau, and S. C. Kot. 2009. "Air Ventilation Impacts of the "Wall Effect" Resulting from the Alignment of High-Rise Buildings." *Atmospheric Environment* 43: 4982–94.